Linear stability analysis of multilayer plane Poiseuille flow

Nitin R. Anturkar, Tasos C. Papanastasiou,[a] and James O. Wilkes
Department of Chemical Engineering, The University of Michigan, Ann Arbor, Michigan 48109

(Received 8 May 1989; accepted 1 December 1989)

A linear stability analysis of n-layer plane Poiseuille flow is performed. Asymptotic solutions are constructed at very small and very large wavenumbers. A numerical analysis is carried out by means of a compound matrix method to identify linearly unstable conditions for wavenumbers of $O(1)$. The governing equations and the boundary conditions are conveniently formulated for n-layer flow. Neutral stability curves are plotted over a broad range of parameters for three-layer flows. The investigated parameters include the viscosity ratios, the flow rate ratios, the density ratios, the interfacial tensions, and the Stokes and Reynolds numbers.

I. INTRODUCTION

Multilayer flows of immiscible liquids are involved in several engineering applications such as in multilayer extrusion of plastic films,[1] in multilayer coating,[2] in lubricated squeezing flows,[3] and in the transportation of oil.[4] At certain processing conditions, wavy interfaces are observed in these multilayer flows—a phenomenon known as *interfacial instability*. In extreme cases, this instability can also cause intermixing of layers.

The interfacial instability in Poiseuille and Couette flows was first investigated by Yih[5] using a linear stability analysis of two-dimensional long-wavelength disturbances. His analytical expressions indicated that the viscosity stratification can induce the interfacial instability at vanishingly small Reynolds numbers. Yiantsios and Higgins[6] extended the analysis to include the effect of an arbitrary wavelength on the stability of two-layer plane Poiseuille flow. The effects of gravity, of interfacial tensions, and of the viscosity, density, and thickness ratios on the stability were studied. In a recent paper, Hooper[7] identified two mechanisms for instability in two-layer plane Poiseuille flow—one mechanism is associated with the presence of the interface, and the other with the presence of the boundary walls. The second type of mechanism is more closely related to shear mode instability of one or more layers and has been addressed in Ref. 6 as well.

Besides the studies on plane Poiseuille flows, linear stability analyses of two-layer axisymmetric Poiseuille flows and Couette flows have been carried out by several researchers.[8–14] A linear stability analysis of multilayer flow on an inclined plane was also carried out[15,16] and results were presented for three-layer and five-layer flows. A theoretical explanation based on the linear stability analysis of axisymmetric multilayer flows is proposed by Hickox[17] and Joseph *et al.*[9] for the experimentally observed phenomenon[18,19] of encapsulation of viscous liquid by the liquid of low viscosity in long pipes. They found that the flow must be linearly unstable for the encapsulation to occur and that the volume ratio is a crucial factor along with the viscosities. Since an arrangement of a thin layer of less viscous liquid at the wall is experimentally favored, Hooper[10] and Renardy[13] particularly studied the effects of a thin layer near the wall on the stability. They also observed that a flow with a thin layer of the more viscous liquid at the walls is always linearly unstable, whereas the stability of a flow with a thin layer of the less viscous liquid at the walls depends on the wavelength of the disturbance. These results agreed with the earlier results of Wang *et al.*[16] The above results are encouraging for practical applications of the thin layers in the transportation of oil and in the lubricated squeezing flows.

While there is a large amount of literature on the stability of multilayer flows, the works on plane Poiseuille flows are limited. Besides, when more than two layers are involved, the role of additional layers on the stability of the flow is not clear. Several engineering applications of multilayer flows, such as multilayer extrusion and multilayer coating, involve more than two layers, and the stability of such flows is of practical interest.[1] In this paper, we formulate the linear stability analysis of n-layer plane Poiseuille flow of Newtonian liquids, where n is arbitrary (Sec. II). Asymptotic solutions are constructed for disturbances of very short and very long wavelengths in Sec. III. However, the dominant mode of instability can be due to a disturbance of a wavelength of order $O(1)$. Therefore, the numerical solution of the corresponding eigenvalue problem at an arbitrary wavelength is also constructed, thereby identifying the neutral stability curves over a wide spectrum of wavelengths (Sec. IV). The neutral stability curves are plotted in the parametric space of the viscosity, density, and flow rate ratios; of interfacial tensions; and of the Reynolds and the Stokes numbers. Although the formulation of the equations is for n-layer flow, we restrict the numerical results to three-layer flow because of the large number of parameters involved in the analysis.

II. GOVERNING EQUATIONS

The flow geometry is shown in Fig. 1 together with a coordinate transformation that simplifies the governing equations. The following dimensionless variables are used:

[a] Correspondence concerning this paper should be addressed to T. C. Papanastasiou.

 0899-8213/90/040530-12$02.00

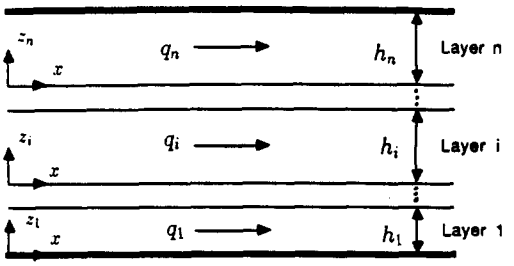

FIG. 1. Geometry of multilayer, plane Poiseuille flow and transformation of the coordinates.

$$x^* = x/H, \quad z_j^* = z_j/H,$$
$$u_j^* = u_j/V, \quad v_j^* = v_j/V, \quad j = 1,2,...,n, \tag{1}$$
$$p^* = p/(\mu_1 V/H), \quad t^* = t/(H/V).$$

The subscript j denotes the jth layer and the asterisk, which is hereafter suppressed, denotes the normalized variables. The variables u and v are the velocity components along the x and the z directions, respectively, t is the time, and p is the pressure. The variables are normalized by the total average velocity V, and by the total thickness H of the channel. The primary flow is a channel flow of parabolic velocity profiles:

$$u_j = A_j + B_j z_j + C_j z_j^2, \quad 0 \leqslant z_j \leqslant h_j, \quad j = 1,2,...,n, \tag{2}$$

where A_j and B_j are constants, $C_j = (1/2m_j)(\partial p/\partial z)$ is the parameter involving the pressure gradient and the viscosity ratio $m_j = \mu_j/\mu_1$, and h_j is the thickness of the jth layer. The flow rates in terms of (2) yield $(3n+1)$ equations for $(3n+1)$ unknowns h_j, A_j, and B_j for each layer, and the pressure p, the common pressure in all the layers. The resulting set of equations consists of the integral continuity equation

$$q_j = A_j h_j + B_j (h_j^2/2) + C_j (h_j^3/3), \quad j = 1,2,...,n; \tag{3a}$$

the no-slip boundary conditions

$$A_1 = 0, \tag{3b}$$
$$A_n + h_n B_n + C_n h_n^2 = 0; \tag{3c}$$

the continuity of velocity and shear stress at the interfaces,

$$A_j + h_j B_j + C_j h_j^2 - A_{j+1} = 0, \quad j = 1,2,...,n-1, \tag{3d}$$
$$B_j + 2C_j h_j - (m_{j+1}/m_j) B_{j+1} = 0, \quad j = 1,2,...,n-1; \tag{3e}$$

and the total thickness of the channel,

$$\sum_{j=1}^{n} h_j = 1. \tag{3f}$$

Note also that $\Sigma_{j=1}^{n} q_j = 1$, where q_j is the dimensionless flow rate in the jth layer. When the thicknesses are specified, the same equations can be solved with the flow rates as the unknowns. However, since the flow rates rather than the thicknesses are the easily measurable quantities under experimental or processing conditions, the equations and the results are presented in terms of flow rates.

Linear stability analysis of two-layer flow is discussed by Yih.[5] We will extend the analysis to n-layer flow, shown in Fig. 1. For two-dimensional disturbances, when primary and secondary flows are decomposed, the disturbed velocities can be represented in the form of streamfunctions $\psi_j(x,z_j,t)$ which satisfy the continuity equation of disturbed velocities automatically. The customary representation of the streamfunctions and the disturbed pressures in the linear stability analysis has an exponential form:

$$(p,\psi_j) = (f(z_j),\phi_j(z_j))\exp[i\alpha(x-ct)], \tag{4}$$

where α is the real wavenumber, $c = c_R + ic_I$ is the complex velocity of the disturbances, and $f(z_j)$ and $\phi_j(z_j)$ are the amplitudes of the disturbances. When $c_I > 0$, the equations are temporally unstable and when $c_I < 0$, they are stable. Neutral stability corresponds to $c_I = 0$. The Orr–Sommerfeld equations are obtained for each layer by substituting (4) into the linearized momentum equations and then eliminating the pressure. The resulting equations are

$$m_j(\phi_j^{IV} - 2\alpha^2\phi_j'' + \alpha^4\phi_j) = i\alpha \,\mathrm{Re}_j[(\phi_j'' - \alpha^2\phi_j)(u_j - c) - u_j''\phi_j], \quad j = 1,2,...,n, \tag{5}$$

where u_j and its derivatives correspond to the primary flow and $\mathrm{Re}_j = \rho_j VH/\mu_1$ are the Reynolds numbers, which can also be expressed as $\mathrm{Re}_j = \mathrm{Re}_1 d_j$, where $d_j = \rho_j/\rho_1$ is the density ratio. The form of the Orr–Sommerfeld equation does not change from layer to layer except that its derivatives, denoted by primes, are evaluated with respect to z_j, the coordinate associated with the respective layer. This general form of the equation for n layers is entirely due to the coordinate transformation (Fig. 1).

The interfacial boundary conditions need to be evaluated at the disturbed locations of the interfaces, which can be expressed in terms of $\phi_j(h_j)$ by means of the kinematic boundary conditions. The no-slip boundary condition at the walls and the Taylor series expansion of the interfacial boundary conditions about the steady-state interfacial locations give rise to the following equations:

no-slip at the walls,

$$\phi_1(0) = \phi_1'(0) = 0, \tag{6a}$$
$$\phi_n(h_n) = \phi_n'(h_n) = 0; \tag{6b}$$

continuity of u_j,

$$\phi_j' + \phi_j u_j'/\tilde{c}_j = \phi_{j+1}' + \phi_{j+1} u_{j+1}'/\tilde{c}_{j+1}, \tag{6c}$$

continuity of v_j,

$$\phi_j = \phi_{j+1}; \tag{6d}$$

continuity of shear stress,

$$m_j(\phi_j'' + \alpha^2\phi_j) = m_{j+1}(\phi_{j+1}'' + \alpha^2\phi_{j+1}); \tag{6e}$$

continuity of normal stress,

$$i\alpha \,\mathrm{Re}_{j+1}(\tilde{c}_{j+1}\phi_{j+1}' + u_{j+1}'\phi_{j+1}) + m_{j+1}(\phi_{j+1}''' - 3\alpha^2\phi_{j+1}') - i\alpha \,\mathrm{Re}_j(\tilde{c}_j\phi_j' + u_j'\phi_j) - m_j(\phi_j''' - 3\alpha^2\phi_j') = [i\alpha^3/\mathrm{Ca}_j + i\alpha \,\mathrm{St}(d_{j+1} - d_j)](\phi_j/\tilde{c}_j); \tag{6f}$$

where $\tilde{c}_j = c - u_j$, and the dimensionless groups $\mathrm{St} = (H^2 g\rho_1)/(V\mu_1)$ and $\mathrm{Ca}_j = V\mu_1/\sigma_j$ are the Stokes number (proportional to gravity g) and the capillary number (inversely proportional to interfacial tension σ_j), respective-

ly. In (6c)–(6f), the variables with subscript j are evaluated at $z_j = h_j$ and the variables with subscript $j+1$ are evaluated at $z_{j+1} = 0$, where $j = 1,2,\ldots, n-1$.

Equations (5) and (6) form an eigenvalue problem with complex velocity of disturbance c (the eigenvalue) and amplitudes of disturbance $\phi_j(z_j)$ (the eigenfunctions). The eigenvalue depends on the parameters α, m_j, q_j, d_j, Re_j, St, and Ca_j. Although in this paper only plane Poiseuille flow is considered, the primary and the secondary flow equations can be used for plane Couette flow and for the combinations of the two by modifying (3b) and (3c) appropriately.

III. ASYMPTOTIC ANALYSIS

A. Long-wavelength analysis ($\alpha \to 0$)

The eigenfunctions and the eigenvalue are expanded as a regular perturbation series of α:

$$\phi_j \simeq \phi_{j,0} + \alpha\phi_{j,1} + O(\alpha^2), \quad j = 1,2,\ldots,n,$$
$$c \simeq c_0 + \alpha c_1 + O(\alpha^2). \tag{7}$$

Equation (7) is substituted in (5) and (6) and terms of the same order of α are collected. The resulting equations are solved sequentially for the coefficients of each order of ϕ_j and c. Since the procedure is standard, only the final form of the equations is listed here.

The zeroth-order solution for the eigenfunctions is

$$\phi_{j,0} = D_{j,0} + E_{j,0}z_j + F_{j,0}z_j^2 + G_{j,0}z_j^3,$$
$$0 \leqslant z_j \leqslant h_j, \quad j = 1,2,\ldots,n, \tag{8}$$

where $D_{j,0}$, $E_{j,0}$, $F_{j,0}$, and $G_{j,0}$ are constants. By substituting (8) in the zeroth-order boundary conditions, $4n$ equations with $4n$ unknowns, $D_{j,0}$, $E_{j,0}$, $F_{j,0}$, and $G_{j,0}$ are obtained:

$$D_{1,0} = 0, \tag{9a}$$
$$E_{1,0} = 0, \tag{9b}$$
$$D_{j,0} + E_{j,0}h_j + F_{j,0}h_j^2 + G_{j,0}h_j^3 - D_{j+1,0} = 0, \tag{9c}$$
$$\tilde{c}_{j,0}(E_{j,0} + 2F_{j,0}h_j + 3G_{j,0}h_j^2) + u_j'(h_j)(D_{j,0} + E_{j,0}h_j + F_{j,0}h_j^2 + G_{j,0}h_j^3) - \tilde{c}_{j+1,0}E_{j+1,0} - D_{j+1,0}B_{j+1} = 0, \tag{9d}$$
$$m_j(2F_{j,0} + 6G_{j,0}h_j) - 2m_{j+1}F_{j+1,0} = 0, \tag{9e}$$
$$m_jG_{j,0} - m_{j+1}G_{j+1,0} = 0, \quad j = 1,2,\ldots,n-1, \tag{9f}$$
$$D_{n,0} + E_{n,0}h_n + F_{n,0}h_n^2 + G_{n,0}h_n^3 = 0, \tag{9g}$$
$$E_{n,0} + 2F_{n,0}h_n + 3G_{n,0}h_n^2 = 0, \tag{9h}$$

where $\tilde{c}_{j,0} = c_0 - u_j(h_j)$. One of the eigenfunctions is conveniently normalized such that $\phi_{1,0}(h_1) = 1$, and therefore

$$D_{1,0} + E_{1,0}h_1 + F_{1,0}h_1^2 + G_{1,0}h_1^3 = 1. \tag{10}$$

Equations (9) and (10) are solved simultaneously to evaluate the unknown coefficients in (8) and the zeroth-order eigenvalue c_0. Gravity appears in the first-order equations, and interfacial tensions in the third-order equations. The solution of (9) and (10) is real, implying that $c_{0i} = 0$. Thus multilayer plane Poiseuille flow is always neutrally stable to the disturbances of infinitely long wavelengths.

The solution of (5) at $O(\alpha)$ is expressed as

$$\phi_{j,1} = D_{j,1} + E_{j,1}z_j + F_{j,1}z_j^2 + G_{j,1}z_j^3 + \chi_j(z_j),$$
$$0 \leqslant z_j \leqslant h_j, \quad j = 1,2,\ldots,n, \tag{11}$$

where

$$\chi_j(z_j) = \frac{U_{j,0}}{24}z_j^4 + \frac{U_{j,1}}{120}z_j^5 + \frac{U_{j,2}}{360}z_j^6 + \frac{U_{j,3}}{840}z_j^7,$$
$$U_{j,0} = (2i\,\mathrm{Re}_j/m_j)(-c_0F_{j,0} + A_jF_{j,0} - C_jD_{j,0}),$$
$$U_{j,1} = (2i\,\mathrm{Re}_j/m_j)(-3c_0G_{j,0} + 3A_jG_{j,0} + B_jF_{j,0} - C_jE_{j,0}),$$
$$U_{j,2} = 6i\,\mathrm{Re}_jB_jG_{j,0}/m_j,$$
$$U_{j,3} = 4i\,\mathrm{Re}_jC_jG_{j,0}/m_j.$$

By substituting the boundary conditions (6) of $O(\alpha)$ in (11), $4n$ equations are obtained:

$$D_{1,1} = 0, \tag{12a}$$
$$E_{1,1} = 0, \tag{12b}$$
$$D_{j,1} + E_{j,1}h_j + F_{j,1}h_j^2 + G_{j,1}h_j^3 + \chi_j(h_j) - D_{j+1,1} = 0, \tag{12c}$$
$$\tilde{c}_{j,0}[E_{j,1} + 2F_{j,1}h_j + 3G_{j,1}h_j^2 + \chi_j'(h_j)] + u_j'(h_j)[D_{j,1} + E_{j,1}h_j + F_{j,1}h_j^2 + G_{j,1}h_j^3 + \chi_j(h_j)] + c_1(E_{j,0} + 2F_{j,0}h_j + 3G_{j,0}h_j^2) - \tilde{c}_{j+1,0}E_{j+1,1} - D_{j+1,1}B_{j+1} - c_1E_{j+1,0} = 0, \tag{12d}$$
$$m_j(2F_{j,1} + 6G_{j,1}h_j + \chi_j''(h_j)) - 2m_{j+1}F_{j+1,1} = 0. \tag{12e}$$
$$6m_{j+1}G_{j+1,1} - 6m_jG_{j,1} - m_j\chi_j'''(h_j) + i\,\mathrm{Re}_{j+1}(c_{j+1,0}E_{j+1,0} + D_{j+1,0}B_{j+1}) - i\,\mathrm{Re}_j\tilde{c}_{j,0}(E_{j,0} + 2F_{j,0}h_j + 3G_{j,0}h_j^2) - i\,\mathrm{St}(d_{j+1} - d_j)\phi_{j,0}/\tilde{c}_{j,0} - i\,\mathrm{Re}_j u_j'(h_j)(D_{j,0} + E_{j,0}h_j + F_{j,0}h_j^2 + G_{j,0}h_j^3) = 0, \tag{12f}$$
$$D_{n,1} + E_{n,1}h_n + F_{n,1}h_n^2 + G_{n,1}h_n^3 + \chi_n(h_n) = 0, \tag{12g}$$
$$E_{n,1} + 2F_{n,1}h_n + 3G_{n,1}h_n^2 + \chi_n'(h_n) = 0, \tag{12h}$$

where $j = 1,2,\ldots, n-1$. The normalization of the eigenfunction $\phi_1(h_1)$ gives

$$D_{1,1} + E_{1,1}h_1 + F_{1,1}h_1^2 + G_{1,1}h_1^3 + \chi_1(h_1) = 0. \tag{13}$$

Equations (12) and (13) provide the necessary equations for evaluating the unknown coefficients of (11) and the first-order eigenvalue c_1. Since the zeroth-order solution is real, the first-order solution is purely imaginary. Therefore, the eigenvalue c_1 is useful in finding the stable and the unstable conditions.

The actual procedure of finding c_1 is first to solve the nonlinear simultaneous equations (3a)–(3f) to obtain the primary flow, then to solve (9) and (10) simultaneously to get the zeroth-order solution, and finally to solve (12) and (13) to get the first-order solution, including c_1. For two-layer flow, analytical expressions have been obtained.[5,6] However, because of the unwieldy algebra involved in deriving analytical expressions for flows with three or more layers, they can best be solved by standard numerical techniques. We used the software package MINPACK, which implements Newton's iteration, to solve the system of nonlinear equations.

The eigenvalue is proportional to the Reynolds number. Therefore, although a nonzero Reynolds number is essential for an unstable flow to exist, the neutral stability curves do not depend on the Reynolds number. In the absence of gravity, the stability results are not altered when the first and the third layers are interchanged by interchanging the viscosity ratios and the flow rate ratios.

The results of the asymptotic analysis of three-layer flow are shown in Figs. 2 and 3 in the form of neutral stability curves in the plane of the viscosity ratio m_2 and the flow rate ratio q_2/q_1. The effects of the flow rate ratio q_3/q_1 and the viscosity ratio m_3 of the third layer on the neutral stability curves of three-layer flow are studied in Fig. 2, whereas the effects of gravity on the neutral stability curves of three-layer flow are studied in Fig. 3. As mentioned earlier, the results are presented in terms of the flow rates rather than the thicknesses, because the flow rates are easily measurable quantities under experimental and processing conditions.

The same liquid in layers 1 and 3 ($m_3 = 1.0$) is considered for the case illustrated in Fig. 2(a) and the effect of the variation in q_3/q_1 on the stability of the flow is studied. This configuration with the same liquid in the outer layers and the high flow rate in the middle layer has applications in lubricated squeezing flows and in the transportation of oil. The neutrally stable conditions are at $\sqrt{m_2} = q_2/q_1$ for two-layer

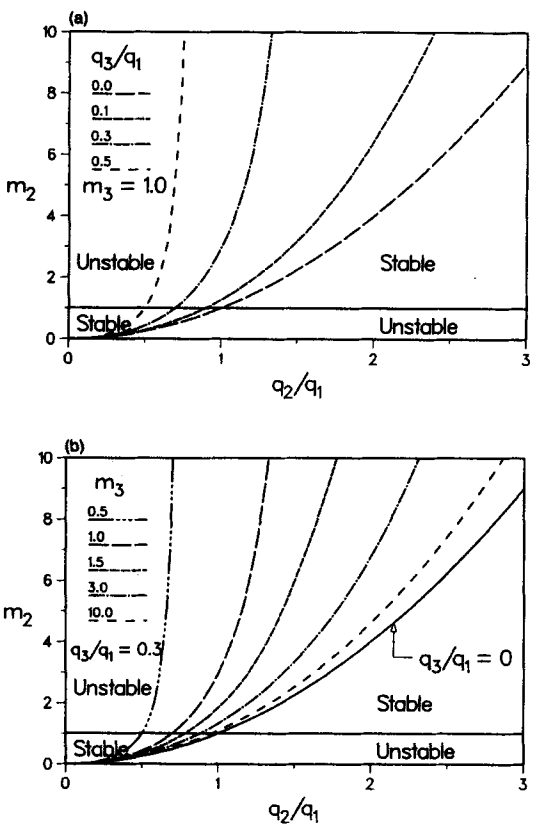

FIG. 2. Neutral stability curves for three-layer flow in the m_2-q_2/q_1 plane at vanishingly small α: (a) for various flow rate ratios q_3/q_1 at viscosity ratio $m_3 = 1.0$, and (b) for various viscosity ratios m_3 at flow rate ratio $q_3/q_1 = 0.3$. The other parameters are the density ratios $d_j = 1.0$, $\mathrm{Re}_j = 5.0$, and $\mathrm{St} = 0.0$.

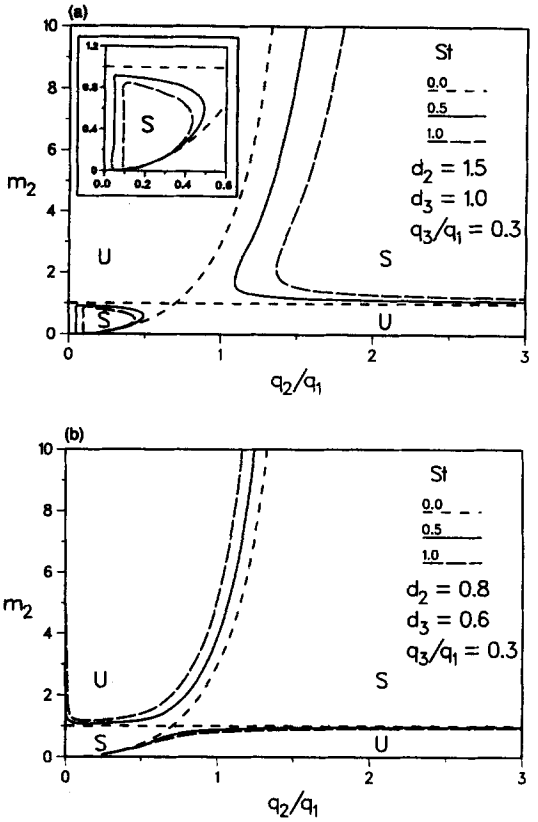

FIG. 3. Effect of gravity on the neutral stability curves for three-layer flow in the m_2-q_2/q_1 plane at vanishingly small α: (a) destabilizing effect when the density ratios are $d_2 = 1.5$ and $d_3 = 1.0$, and (b) stabilizing effect when the density ratios are $d_2 = 0.8$ and $d_3 = 0.6$. The other parameters are the viscosity ratio $m_3 = 1.0$, the flow rate ratio $q_3/q_1 = 0.3$, and $\mathrm{Re}_j = 5.0$. Stable and unstable regions are denoted by S and U, respectively.

flow ($q_3/q_1 = 0.0$). Since it can be shown that $q_2/q_1 = h_2/h_1$ at $\sqrt{m_2} = q_2/q_1$, our results agree with the results reported by Yiantsios and Higgins[6] for two-layer flow. For each q_3/q_1, there are *two* neutral stability curves that separate the stable regions from the unstable regions. The neutral stability curve corresponding to $m_2 = 1.0$ remains the same for various q_3/q_1, whereas the other neutral stability curve is strongly affected by the variation in q_3/q_1. The increasing flow rate in the third layer from $q_3/q_1 = 0$ to 1 is stabilizing when a more viscous liquid is in the second layer ($m_2 > 1$) and is destabilizing when a less viscous liquid is in the second layer ($m_2 < 1$), whereas, when liquids in all layers have the same viscosity ($m_2 = 1$), the flow is neutrally stable. At $q_3/q_1 = 1$, the system is always stable for $m_2 > 1$ and is always unstable for $m_2 < 1$ for long wave disturbances. These results appear to agree with the encapsulation observed in experiments.[18,19] A theoretical explanation based on linear stability analyses of axisymmetric flows[9,17] suggested that the flow must be linearly unstable for the encapsulation to occur and that the volume ratio is a crucial factor along with the viscosities. Although the two-dimensional plane Poiseuille flow is considered here, the results are similar to Joseph *et al.*[9] At low flow rate ratios q_2/q_1, the flow is unstable for $m_2 > 1$ when q_3/q_1 is small. In fact, in plane Poiseuille flow, the flow

rate of each individual layer (rather than their summation $q_1 + q_3$) contributes in determining the stability of the flow.

In Fig. 2(b), the neutral stability curves are plotted for various values of m_3 in an nonsymmetric flow configuration of $q_3/q_1 = 0.3$. This configuration is encountered when recycled plastic scrap is introduced only in one of the outer layers in the food-packaging industry, thereby creating nonsymmetric flow with different viscosities in the outer layers ($m_3 \neq 1.0$). As m_3 increases, the neutral stability curve approaches the curve for $q_3/q_1 = 0$, because as $m_3 \to \infty$, the third layer acts as a rigid wall. However, as $m_3 \to 0$, $h_3 \to 1$ and the flow becomes a free surface flow in the presence of very thin first and second layers. In this situation, the flow is always unstable for $m_2 < 1$ and is always stable for $m_2 > 1$.

The gravitational force can have a stabilizing or a destabilizing effect, depending on the density ratios, as shown in Fig. 3. When the layers are arranged in such a way that the liquids with higher densities occupy lower layers, the gravitational force stabilizes the flow [Fig. 3(b)], whereas in other configurations, the gravitational force destabilizes the flow [e.g., in Fig. 3(a)]. Note that (12f) is singular at $\tilde{c}_{j,0} = 0$. In our calculations, this singularity is encountered at $m_2 = 1$, and the eigenvalues cannot be evaluated at these singular points. However, the eigenvalues at $m_2 = 1$ are not essential in calculating neutral stability curves. In the neighborhood of the singular points, the eigenvalues can be estimated without loss of accuracy because of substantially large values of $\tilde{c}_{1,0}$ at these points [for example, at $m_2 = 0.99$, $c_{1,0} = O(10^{-3})$ at $q_3/q_1 = 0.3$, $d_i = 1$, and $\mathrm{Re}_i = 5$]. Computations with single and double precision matched up to four decimal points, further confirming the accuracy of the calculations.

B. Short-wavelength analysis ($\alpha \to \infty$)

The asymptotic analysis for disturbances with short wavelengths is carried out following Hooper and Boyd.[8] To analyze the stability locally near the interface, the flow coordinates (x,z_j) are stretched by the scale of the wavelength such that the rescaled coordinates (X,Z_j) are

$$X = \alpha x, \quad \text{and} \quad Z_j = \alpha z_j. \tag{14}$$

The rescaled form of the Orr–Sommerfeld equations along with the *interfacial* boundary conditions form the eigenvalue problems for each interface separately, and provide the solutions valid at the scale of the wavelength but uniformly valid in z_j.

Asymptotic expansions of the form

$$\phi_j = \left(\phi_{j,0} + \frac{\phi_{j,1}}{\alpha} + \frac{\phi_{j,2}}{\alpha^2} + \frac{\phi_{j,3}}{\alpha^3} + \cdots\right)\exp(-Z_{j+1}),$$

$$\phi_{j+1} = \left(\phi_{j+1,0} + \frac{\phi_{j+1,1}}{\alpha} + \frac{\phi_{j+1,2}}{\alpha^2} + \frac{\phi_{j+1,3}}{\alpha^3} + \cdots\right) \times \exp(Z_{j+1}),$$

$$c_j = c_{j,0} + \frac{c_{j,1}}{\alpha}\frac{c_{j,2}}{\alpha^2} + \frac{c_{j,3}}{\alpha^3} + \cdots, \quad j = 1,2,\ldots,n-1, \tag{15}$$

where c_j is the eigenvalue at the jth interface, are appropriate. The exponential terms are not necessary but convenient. The coordinate transformation is carried out for each ϕ_j, such that the new coordinate is located at the jth interface. Since the base velocity was linear in Ref. 8, the expansion was in even powers of the inverse of the wavenumber. In this analysis, however, all the powers of the inverse of the wavenumber are needed because of the parabolic velocity profiles.[6,8,14]

When the gravitational force and interfacial tensions are neglected, the expression for the eigenvalue is

$$c_j = A_{j+1} + \frac{5i\,\mathrm{Re}_j B_{j+1}^2}{2(m_j + m_{j+1})^2 m_j^2}\left(\frac{d_{j+1}}{d_j} m_j^2 - m_{j+1}^2\right) \times (m_j - m_{j+1})\alpha^{-3} + O(\alpha^{-4}), \tag{16}$$

where $j = 1,2,\ldots,n-1$. The above expression shows that the system is unstable to short-wave disturbances for nonzero Re_j and nonzero B_{j+1} unless $(d_{j+1}/d_j) > (m_{j+1}/m_j)^2 > 1$ or $(d_{j+1}/d_j) < (m_{j+1}/m_j)^2 < 1$. Unlike the long-wavelength asymptotic analysis, the density ratios play a major role in the stability analysis, even for negligible gravitational force. The disturbances are localized only at the interfaces, and, for complete stability, each of the interfaces should be stable.

For various orders of magnitudes of interfacial tensions and the gravitational force, the perturbation solution for the eigenvalues is

$$\frac{\alpha}{\mathrm{Ca}_j} = \frac{\mathrm{St}(d_{j+1} - d_j)}{\alpha} = O(1):$$

$$c_j = A_{j+1} - \frac{i[(\alpha/\mathrm{Ca}_j) + (\mathrm{St}/\alpha)(d_{j+1} - d_j)]}{2(m_j + m_{j+1})}\alpha^{-1} + O(\alpha^{-2}),$$

$$\frac{1}{\mathrm{Ca}_j} = \frac{\mathrm{St}(d_{j+1} - d_j)}{\alpha^2} = O(1):$$

$$c_j = A_{j+1} - \frac{[1/\mathrm{Ca}_j + (\mathrm{St}/\alpha^2)(d_{j+1} - d_j)]}{2(m_j + m_{j+1})} + O(\alpha^{-1}). \tag{17}$$

The stabilizing effect of the interfacial tension enters at the lowest possible order of the inverse of α, indicating the strong influence of the interfacial tension compared to the effects of the other terms. The destabilizing effect of gravity, however, competes with the stabilizing effect of the interfacial tension when $d_j > d_{j+1}$. The Stokes number must be two order of magnitudes larger than the inverse of the capillary number Ca_j for the gravitational term to become as important as the interfacial tension, when $(d_{j+1} - d_j) = O(1)$. When $d_j < d_{j+1}$, the gravitational force stabilizes the flow.

IV. NUMERICAL ANALYSIS

The asymptotic analysis fails to predict the neutral stability curves when the wavelength of a disturbance is of $O(1)$. However, the dominant mode of the instability can be of a wavelength of $O(1)$. Therefore, to obtain the stability results over a wide range of wavelengths, a numerical solution of the Orr–Sommerfeld equations and boundary conditions is undertaken. Several methods are available to determine the eigenvalue c in terms of the parameter space of α,

q_j/q_1, Re_j, d_j, m_j, Ca_j, and St. For small wavenumbers and Reynolds numbers ($\alpha < 5.0$, $\mathrm{Re}_j < 200$), most of these methods are accurate. However, at large wavenumbers and large Reynolds numbers, the eigenvalue problem of (5) and (6) becomes numerically stiff. The compound matrix method,[20,21] which is accurate for stiff systems,[22] was implemented. However, it had to be modified to accommodate several interfacial boundary conditions for n-layer flow.

The compound matrix method can only compute one eigenvalue for a given set of parameters and the solution depends on the initial guess provided for the eigenvalue. Therefore, for the method to converge to the most dominant mode, the asymptotic solutions are used for obtaining the initial guess. The eigenvalues in the complete domain of the parameter space are then obtained by first-order continuation to provide the initial guess. The asymptotic solutions at $\alpha \to 0$ are compared with the numerical results in Tables I and II, for $\mathrm{St} = 0$ and $\mathrm{St} \neq 0$, respectively. For a set of representative values of parameters, the wave speeds calculated by these two methods agree well for $\alpha = 0.001$ for various values of q_3/q_1, and deviate marginally as α increases from 0.001 to 0.1.

The asymptotic analysis reveals that the multilayer flow can be unstable to the interfacial disturbances at small Reynolds numbers. In this paper, we investigate this interfacial instability and carry out all our calculations at $\mathrm{Re}_j < 10$, which is typical for industrial processes of multilayer flows such as coating and coextrusion. As a result of the large number of parameters involved in the analysis, results will be presented only for two- and three-layer flows. However, the algorithm can be used for any number of layers.

All the numerical results are presented in the form of neutral stability curves in the α-q_2/q_1 plane. Although the effect of the viscosity ratio m_2 on the neutral stability curves of two-layer flow is studied in Fig. 4, all other results are related to the stability of three-layer flows. The neutral stability curves are considerably affected by the presence of the third layer. In Fig. 5, the effect of the variation in the flow rate ratio q_3/q_1 is investigated for $m_3 = 1.0$, whereas in Fig. 6, the effect of the variation in the viscosity ratio m_3 is investigated for $q_3/q_1 = 0.2$. Similar to the asymptotic analysis, the studies of the above two cases are motivated by their industrial applications in lubricated squeezing flows and in the transportation of oil (Fig. 5), and in the use of the recycled plastic scrap in only one of the outer layers for the food-packaging industry (Fig. 6). The effect of the Stokes number is studied in Figs. 7 and 8, and the effect of the capillary number is studied in Fig. 10 for representative cases. When the Stokes number and the capillary number stabilize the flow, the stable regions at *all* α are identified, and the critical parameters defining these stable regions are plotted in Figs. 9 and 11, respectively.

The neutral stability curves for two-layer flow are shown in Fig. 4 in the α-q_2/q_1 plane for the more viscous liquid in the second layer, such that $m_2 = 5.0$ in Fig. 4(a) and $m_2 = 20.0$ in Fig. 4(b). Interfacial tension and gravity are neglected ($\mathrm{Ca}_1 = \infty$ and $d_2 = 1.0$). For each viscosity ratio m_2, there are two neutral stability curves. The neutral stability curve in the form of a straight line of constant q_2/q_1 at *all* α corresponds exactly to the asymptotic solution $(q_2/q_1)_{as}$ at $\alpha \to 0$ [see Fig. 2(a)]. From Sec. III A, the long-wavelength asymptotic solution for two-layer flow is $(q_2/q_1)_{as} = \sqrt{m_2}$. For $q_2/q_1 > \sqrt{m_2}$, the flow is unstable for large α and stable for small α. The wavenumber at which this demarcation occurs decreases with increasing m_2. For $q_2/q_1 < \sqrt{m_2}$, the flow is unstable for long waves (small α). In addition, there is a region in the form of an envelope at large α in which the flow is stable. A flow rate ratio, $(q_2/q_1)_c$, associated with each envelope, below which the flow is unstable to all wavenumbers, increases with increasing m_2. The extent of the stable region decreases for very large α, such that at $\alpha \gg 1$, the flow is unstable everywhere except at $q_2/q_1 = \sqrt{m_2}$. When $d_2 = 1$, gravity does not influence the stability. Therefore, the neutral stability curves are not altered by inverting m_2 and q_2/q_1 simultaneously. The results in Fig. 4 are similar to the results in Refs. 6 and 7.

For two-layer flow, the effects of a thin layer near the wall are analyzed in Couette and axisymmetric Poiseuille flow.[9,10,13] It is observed that a flow with a thin layer of the

TABLE I. Comparison between the asymptotic solutions at $\alpha \to 0$ and the numerical solutions at small α at various q_2/q_1, for $\mathrm{Re}_j = 5.0$, $\mathrm{Ca}_j = \infty$, $q_3/q_1 = 0.2$, $m_2 = 20.0$, $m_3 = 1.0$, $d_j = 1.0$, and $\mathrm{St} = 0.0$.

q_2/q_1	0.5	1.0
Asymptotic solution	$1.499\,906\,56 + 0.941\,602\,76 \times 10^{-2}\alpha i$	$1.433\,202\,03 + 0.557\,991\,32 \times 10^{-2}\alpha i$
$\alpha = 0.001$	$1.499\,906\,58 + 0.941\,602\,76 \times 10^{-5} i$	$1.433\,201\,99 + 0.557\,991\,32 \times 10^{-5} i$
$\alpha = 0.01$	$1.499\,888\,10 + 0.941\,372\,63 \times 10^{-4} i$	$1.433\,191\,81 + 0.557\,889\,03 \times 10^{-4} i$
$\alpha = 0.1$	$1.498\,053\,37 + 0.918\,662\,56 \times 10^{-3} i$	$1.432\,180\,33 + 0.547\,764\,12 \times 10^{-3} i$
q_2/q_1	2.0	4.0
Asymptotic solution	$1.255\,362\,21 + 0.160\,287\,51 \times 10^{-3}\alpha i$	$1.032\,401\,54 - 0.183\,024\,45 \times 10^{-2}\alpha i$
$\alpha = 0.001$	$1.255\,362\,19 + 0.160\,287\,49 \times 10^{-6} i$	$1.032\,401\,57 - 0.183\,024\,46 \times 10^{-5} i$
$\alpha = 0.01$	$1.255\,361\,93 + 0.160\,272\,64 \times 10^{-5} i$	$1.032\,404\,00 - 0.183\,018\,60 \times 10^{-4} i$
$\alpha = 0.1$	$1.255\,336\,07 + 0.158\,795\,19 \times 10^{-4} i$	$1.032\,635\,37 - 0.182\,434\,13 \times 10^{-3} i$

TABLE II. Comparison between the asymptotic solutions at $\alpha \to 0$ and the numerical solutions at small α at various q_2/q_1 for $\mathrm{Re}_j = 5.0$, $\mathrm{Ca}_j = \infty$, $q_3/q_1 = 0.2$, $m_2 = 20.0$, $m_3 = 1.0$, $d_2 = 1.5$, $d_3 = 1.0$, and $\mathrm{St} = 1.0$.

q_2/q_1	0.5	1.0
Asymptotic solution	$1.499\,906\,56 + 0.129\,303\,15\times10^{-1}\alpha i$	$1.433\,202\,03 + 0.812\,593\,12\times10^{-2}\alpha i$
$\alpha = 0.001$	$1.499\,906\,57 + 0.129\,203\,20\times10^{-4} i$	$1.433\,201\,99 + 0.812\,592\,34\times10^{-5} i$
$\alpha = 0.01$	$1.499\,888\,06 + 0.129\,175\,67\times10^{-3} i$	$1.433\,191\,79 + 0.812\,469\,37\times10^{-4} i$
$\alpha = 0.1$	$1.498\,048\,71 + 0.126\,457\,94\times10^{-2} i$	$1.432\,177\,93 + 0.800\,292\,02\times10^{-3} i$
q_2/q_1	2.0	4.0
Asymptotic solution	$1.255\,362\,21 + 0.143\,858\,93\times10^{-3}\alpha i$	$1.032\,401\,54 - 0.118\,395\,73\times10^{-2}\alpha i$
$\alpha = 0.001$	$1.255\,362\,19 + 0.143\,858\,71\times10^{-6} i$	$1.032\,401\,57 - 0.118\,395\,46\times10^{-5} i$
$\alpha = 0.01$	$1.255\,361\,92 + 0.143\,853\,45\times10^{-5} i$	$1.032\,403\,89 - 0.118\,390\,31\times10^{-4} i$
$\alpha = 0.1$	$1.255\,335\,56 + 0.143\,330\,60\times10^{-4} i$	$1.032\,635\,27 - 0.117\,875\,91\times10^{-3} i$

more viscous liquid is always linearly unstable, whereas a flow with a thin layer of the less viscous liquid depends on the wavenumber α. Our calculations on plane Poiseuille flow are similar to their observations and are relevant to the industrial applications mentioned above.

The neutral stability curves are considerably influenced by the presence of the third layer. In Fig. 5, the neutral stability curves for various flow rate ratios q_3/q_1 are plotted in the α-q_2/q_1 plane for $m_2 = 20.0$ and $m_3 = 1.0$. Interfacial tensions and gravity are neglected. Similar to Fig. 4, there are two neutral stability curves for each q_3/q_1. The neutral stability curve in the form of a straight line of constant q_2/q_1 at *all* α corresponds exactly to the asymptotic solution $(q_2/q_1)_{as}$ at $\alpha \to 0$, and its value decreases with increasing q_3/q_1. When $q_2/q_1 > (q_2/q_1)_{as}$, the flow is unstable for large α and stable for small α. The wavenumber at the transition from the stable region to the unstable region decreases with increasing q_3/q_1 and finally approaches a constant value for $q_3/q_1 \geqslant 0.3$. At $q_2/q_1 < (q_2/q_1)_{as}$, the envelope separating the stable region from the unstable region expands and $(q_2/q_1)_c$ of each envelope decreases as q_3/q_1 increases. As shown in Fig. 5(b), an additional stable region is also observed at small q_2/q_1 and large α, for $q_3/q_1 = 0.1$. At $\alpha \gg 1$, the stable regions degenerate to the lines $q_2/q_1 = 0.0$ and $q_2/q_1 = (q_2/q_1)_{as}$, respectively, and the flow is unstable everywhere except at $q_2/q_1 = 0$ and at $q_2/q_1 = (q_2/q_1)_{as}$. The stable region at low q_2/q_1 and large α expands as q_3/q_1 increases, and as shown in Fig. 5(d), both the stable regions merge together at $q_3/q_1 = 0.17$. Similar merging of the stable regions is also observed at various other conditions as shown in Figs. 6–8 and 10. For $q_3/q_1 > 0.17$, the "combined" stable region expands with increasing q_3/q_1.

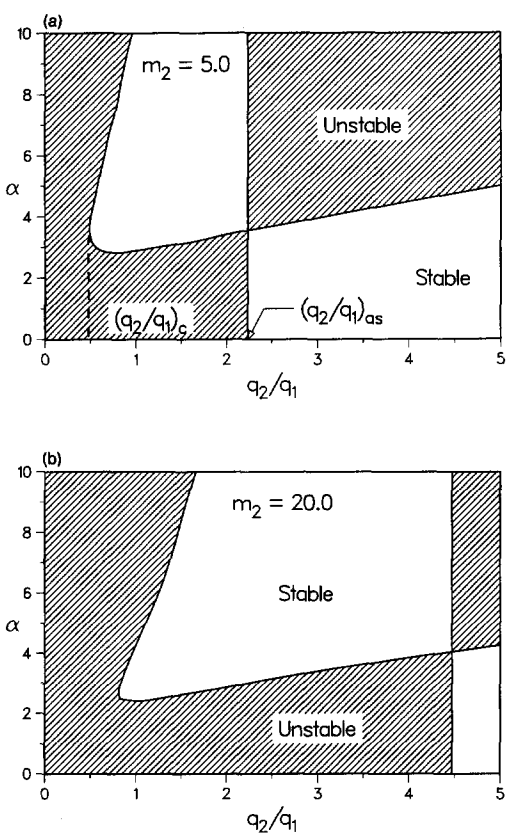

FIG. 4. The neutral stability curves for two-layer flow in the α-q_2/q_1 plane for (a) $m_2 = 5.0$, and (b) $m_2 = 20.0$. The other parameters are the density ratio $d_2 = 1.0$, $\mathrm{Re}_1 = 5.0$, and $\mathrm{St} = 0.0$. The hatched regions are unstable and the unhatched regions are stable.

For $q_3/q_1 \geqslant 0.2$ [see Figs. 5(e)–5(g)], a new feature of the neutral stability curve is observed. A separate unstable region within the stable region is identified. This unstable region decreases as q_3/q_1 increases. Our calculations show that, as q_3/q_1 increases beyond 0.3, the unstable region within the stable region vanishes and the stable region itself expands at the expense of the unstable region at large α and small q_2/q_1. The change in the neutral stability curve for $q_3/q_1 > 0.3$ at low α or at low q_2/q_1 is minimal. Thus, in the presence of the third layer, the stable region expands at low q_2/q_1, whereas at high q_2/q_1 the change in the stable and unstable regions is minimal.

In the absence of gravity, the same neutral stability curves are recovered by interchanging the flow rate ratios and the viscosity ratios of layers 1 and 3. Therefore, for a given m_2, it is sufficient to find the neutral stability curves from $q_3/q_1 = 0$ up to $q_3/q_1 = 1.0$ at $m_3 = 1.0$.

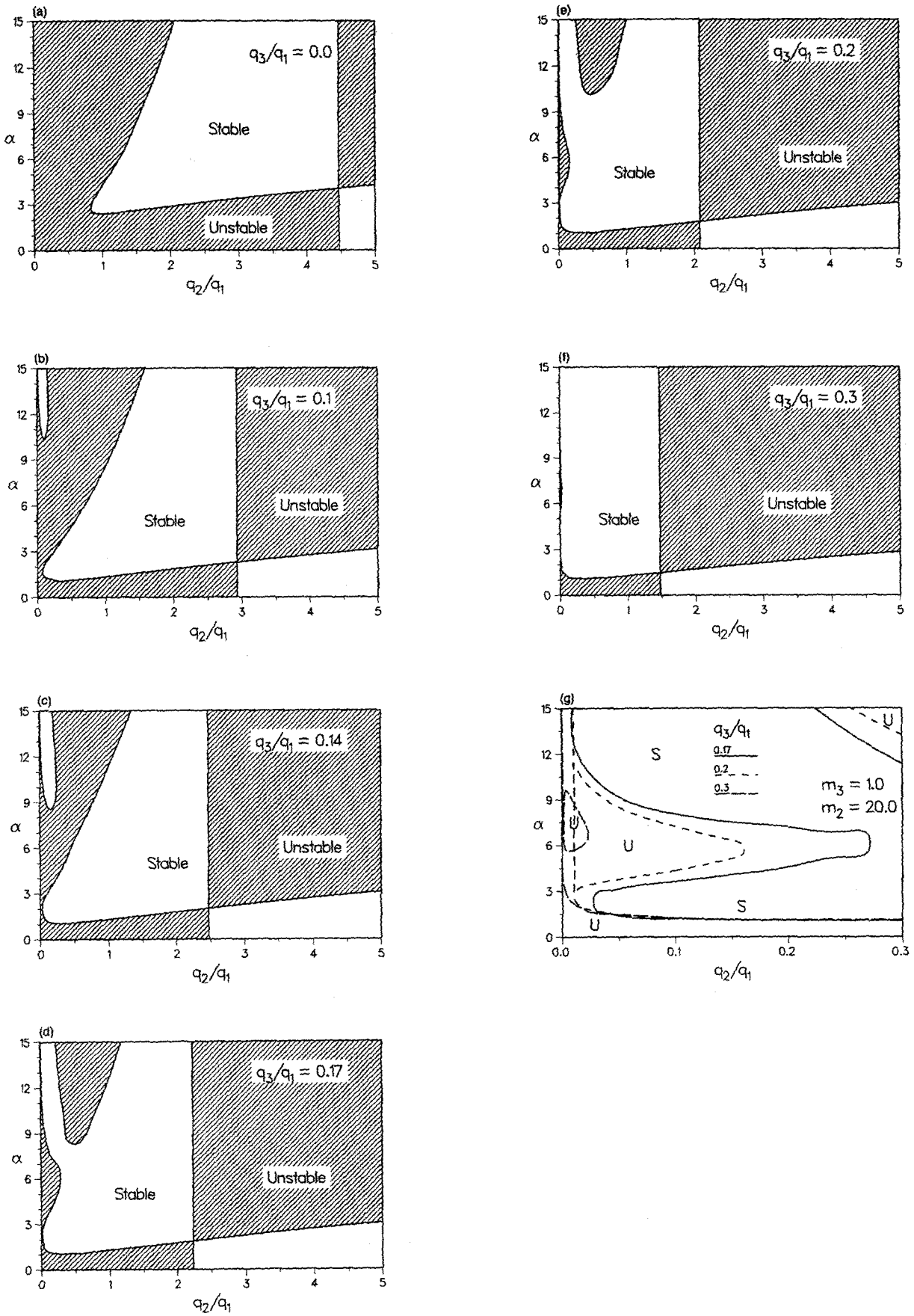

FIG. 5. The neutral stability curves for three-layer flow in the α-q_2/q_1 plane for various flow rate ratios q_3/q_1. From (a) to (f), the flow rate ratio q_3/q_1 is gradually increased from 0.0 to 0.3. In (g), (d)–(f) are stretched along the direction of q_2/q_1. The other parameters are the density ratio $d_j = 1.0$, viscosity ratios $m_2 = 20.0$ and $m_3 = 1.0$, St = 0.0, $\mathrm{Re}_1 = 5.0$, and $\mathrm{Ca}_j = \infty$. The hatched regions are unstable and the unhatched regions are stable, also denoted by U and S, respectively.

At $q_2/q_1 \ll 1$, the instability prevails at $m_2 = 20.0$. However, as q_3/q_1 increases, the region of instability at $q_2/q_1 \ll 1$ shrinks. Thus a very thin middle layer of more viscous liquid is always stable when $m_3 = 1.0$. Note that, at $q_2/q_1 = 0$, the flow is neutrally stable. These results are similar to the results obtained by Joseph *et al.*[9] for axisymmetric two-layer Poiseuille flow.

The neutral stability curves for various m_3 at $q_3/q_1 = 0.2$ are shown in Fig. 6. For negligible interfacial tensions and gravity, the change in the neutral stability curves due to increasing m_3 is found to be qualitatively similar to the change in the neutral stability curves due to increasing q_3/q_1, which is discussed in the previous paragraphs.

Until now, we have not considered the effect of the Reynolds number on the neutral stability curves. At $\mathrm{Re}_j = 0.0$, the flow is always neutrally stable. At low Re_j, the wave speed c is proportional to Re_1 for $d_j = 1.0$. Therefore, although the Reynolds numbers do not contribute to the parameter space where the neutral stability curves are defined, nonzero Reynolds numbers are essential for the interfacial instability to exist in multilayer flow. It was found that, for all $\mathrm{Re}_j < 10$, the wave speed is proportional to Re_j at all α, and therefore the neutral stability curves are not appreciably altered, whereas, for $\mathrm{Re}_j > 10$, the proportionality no longer exists and the flow is more unstable at high Reynolds numbers than at low Reynolds numbers. The effect of the Reynolds number and the transition from the interfacial to the shear modes were systematically investigated by Hooper.[7] Our analysis in this paper is, however, for Reynolds numbers below 10, which are common with highly viscous liquids.

To investigate the effect of gravity, we have computed the neutral stability curves for various Stokes numbers (see Figs. 7 and 8). In Fig. 7, the destabilizing effect of gravity is shown for $d_2 = 1.5$ and $d_3 = 1.0$, whereas in Fig. 8, the stabilizing effect of gravity is shown for $d_2 = 0.8$ and $d_3 = 0.6$. In both cases, the other parameters are $\mathrm{Re}_1 = 5.0$, $\mathrm{Ca}_j = \infty$, $m_2 = 20.0$, $m_3 = 1.0$, and $q_3/q_1 = 0.2$. From Sec. III A, at $\alpha \to 0$, gravity influences the stability through $O(\alpha)$ terms.

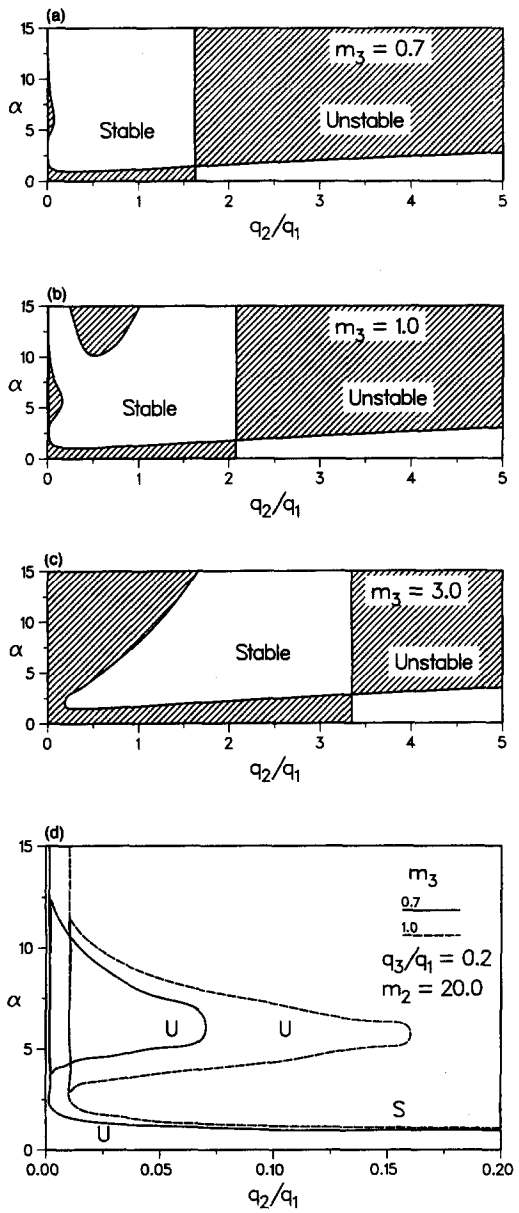

FIG. 6. The neutral stability curves for three-layer flow in the α-q_2/q_1 plane for various viscosity ratios m_3. In (d), Figs. 6(b) and 6(c) are stretched along the direction of the flow rate ratio q_2/q_1. The other parameters are the density ratio $d_j = 1.0$, the viscosity ratio $m_2 = 20.0$, the flow rate ratio $q_3/q_1 = 0.2$, $\mathrm{St} = 0.0$, $\mathrm{Re}_1 = 5.0$, and $\mathrm{Ca}_j = \infty$. The hatched regions are unstable and the unhatched regions are stable, also denoted by U and S, respectively.

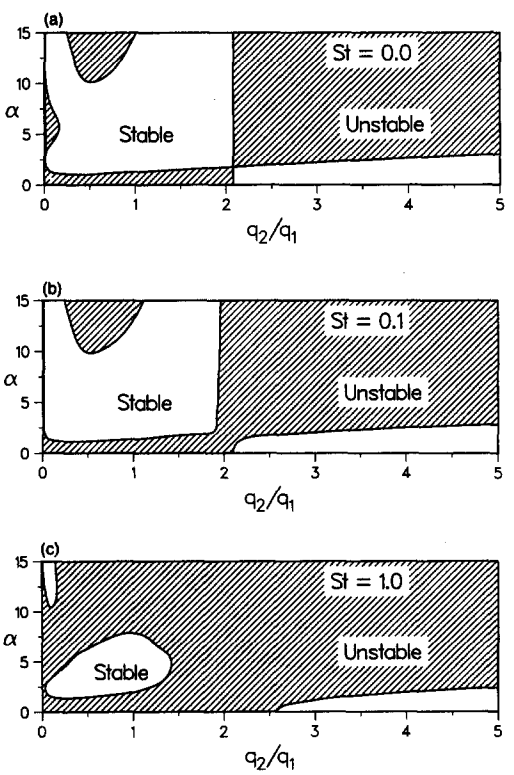

FIG. 7. The destabilizing effect of gravity on the neutral stability curves in three-layer flow in the α-q_2/q_1 plane. The density ratios are $d_2 = 1.5$ and $d_3 = 1.0$. The other parameters are the viscosity ratios $m_2 = 20.0$ and $m_3 = 1.0$, the flow rate ratio $q_3/q_1 = 0.2$, $\mathrm{Re}_1 = 5.0$, and $\mathrm{Ca}_j = \infty$. The hatched regions are unstable and the unhatched regions are stable.

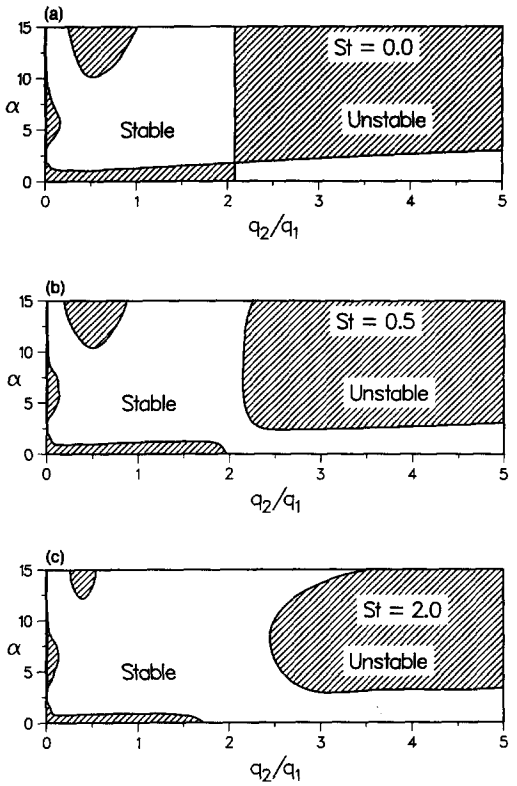

FIG. 8. The stabilizing effect of gravity on the neutral stability curves in three-layer flow in the α-q_2/q_1 plane. The density ratios are $d_2 = 0.8$ and $d_3 = 0.6$. The other parameters are the viscosity ratios $m_2 = 20.0$ and $m_3 = 1.0$, the flow rate ratio $q_3/q_1 = 0.2$, $\mathrm{Re}_1 = 5.0$, and $\mathrm{Ca}_j = \infty$. The hatched regions are unstable and the unhatched regions are stable.

Numerically, the same influence is observed at small α. The effect of gravity is stabilizing (Fig. 8) or destabilizing (Fig. 7) as $\alpha \to 0$, depending on the density ratios of the layers, as in the long-wavelength asymptotic analysis.

In addition, when α is of $O(1)$, the unstable regions grow at the expense of the stable regions, when the density ratios are unfavorable for stability, as shown in Fig. 7. At small α and small q_2/q_1, the effect of St is negligible. However, at large α and small q_2/q_1, the unstable regions grow to the extent that, at St = 1.0, they separate the stable region into two parts: one part is at large α and small q_2/q_1, and the other is in the form of a closed region. Recall that the stable region at large α and small q_2/q_1 is similar to the one observed at lower q_3/q_1 in the absence of gravity [see Fig. 5(b)].

Figure 8 shows the stabilizing effect of gravity at $\alpha \simeq O(1)$. The effect of St is negligible for small q_2/q_1. There are two critical flow rate ratios q_2/q_1 for each St, within which the system is stable for all α; and, as St increases, the distance between the two critical flow rate ratios increases. Note also that the lower critical flow rate ratio corresponds to the long-wavelength asymptotic solution. These critical flow rate ratios q_2/q_1 are plotted against the Stokes number in Fig. 9 to identify the stable regions at *all* α. A similar stabilizing effect of St is also observed for various other values of q_3/q_1.

The effect of interfacial tensions is illustrated in Fig. 10

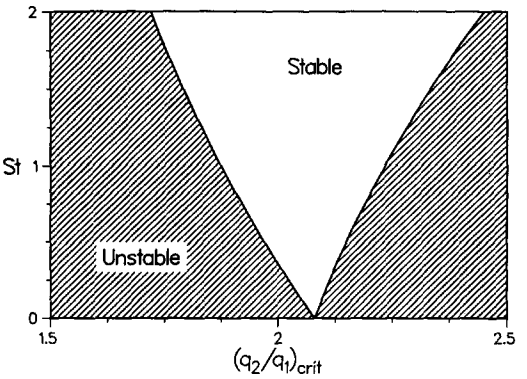

FIG. 9. Diagram of stable conditions at *all* α for three-layer flow in the St-q_2/q_1 plane. The critical values of q_2/q_1 for a given St are obtained from Fig. 8. The other parameters are the viscosity ratios $m_2 = 20.0$ and $m_3 = 1.0$, the density ratios $d_2 = 0.8$ and $d_3 = 0.6$, the flow rate ratio $q_3/q_1 = 0.2$, $\mathrm{Ca}_j = \infty$, and $\mathrm{Re}_1 = 5.0$. The hatched regions are unstable and the unhatched regions are stable.

for $\mathrm{Re}_1 = 5.0$, $q_3/q_1 = 0.2$, $m_2 = 20.0$, $m_3 = 1.0$, $d_j = 1.0$, and St = 0.0. The same liquid is in layers 1 and 3. Interfacial tensions are significant at the small wavenumber asymptotic analysis only through terms of $O(\alpha^3)$. In Fig. 10, at $\alpha \to 0$, the neutral stability curves remain unaltered for various values of interfacial tensions, thus confirming the results of the long-wavelength asymptotic analysis. The asymptotic analysis for large wavenumbers indicates that interfacial tensions play a major role in stabilizing the flow at large α. Figure 10 confirms this observation. In addition, interfacial tensions are also stabilizing for $\alpha \simeq O(1)$; at large flow rate ratios q_2/q_1, the effect of interfacial tensions is dramatic. Similar to Fig. 8, there are two critical flow rate ratios q_2/q_1 for each set of values of the capillary numbers Ca_1 and Ca_2 within which the system is stable for all α. Although the lower critical value of q_2/q_1, obtained by the asymptotic analysis at small wavenumbers, remains unaltered with decreasing Ca_1 and Ca_2, the upper critical value of q_2/q_1 increases rapidly. The critical flow rate ratios q_2/q_1 are plotted against $1/\mathrm{Ca}_j$ (proportional to interfacial tensions) in Fig. 11 for various values of q_3/q_1. The stabilizing effect of interfacial tensions is maximum at $q_3/q_1 = 0.0$ and, with increasing q_3/q_1, this effect gradually decreases.

V. SUMMARY

A linear stability analysis of multilayer channel flow of Newtonian liquids to two-dimensional disturbances has been conducted. The governing equations and the boundary conditions for n-layer flow have been simplified by means of a convenient coordinate transformation that enhances algebraic simplicity. The asymptotic solutions are constructed for the long and short wavelengths and the numerical solutions are computed for the wavelengths of $O(1)$.

The long-wavelength asymptotic analysis suggests that nonsymmetric arrangements, with the thinner material in the outer layers and the thicker material in the middle layer, tend to be more unstable than symmetric arrangements of the same materials. Gravity is found to be always destabilizing, except when the densities are increasing along the direc-

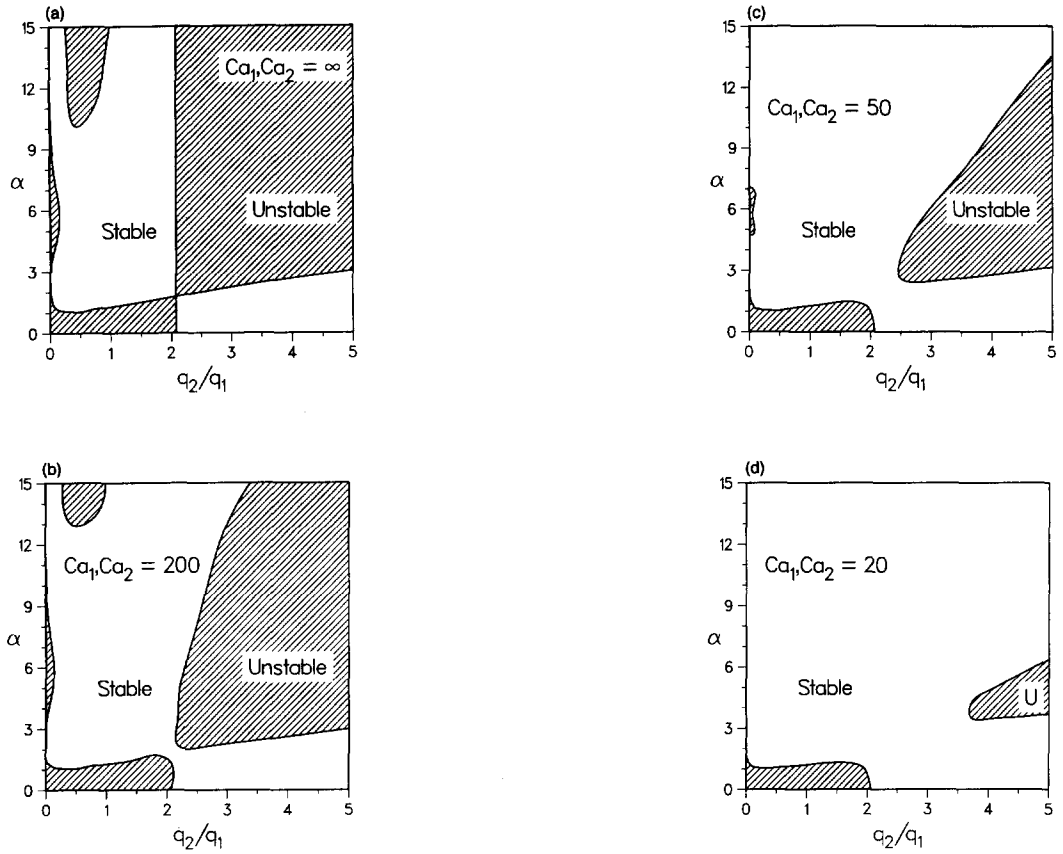

FIG. 10. The stabilizing effect of interfacial tensions on the neutral stability curves in three-layer flow in the α-q_2/q_1 plane. The material properties are the same for layers 1 and 3. The other parameters are the viscosity ratios $m_2 = 20.0$ and $m_3 = 1.0$, the flow rate ratio $q_3/q_1 = 0.2$, the density ratios $d_j = 1.0$, $\mathrm{Re}_1 = 5.0$, and $\mathrm{St} = 0.0$. The hatched regions are unstable and the unhatched regions are stable.

tion of gravity. Interfacial tensions do not play a significant role at long-wavelength disturbances. For disturbances of small wavelengths, however, interfacial tensions stabilize the flow (in some cases, even when the density ratios are unfavorable).

Several new features of the neutral stability curves over a wide range of wavelengths emerge as a result of the presence of the third layer. The flow with the more viscous liquid in the middle layer tends to be stable when q_2/q_1 is small; at large q_2/q_1, it can be stable or unstable, depending on the wavenumber α. The effects of interfacial tensions and of gravity at $\alpha \simeq O(1)$ agree with the results of the asymptotic analysis at $\alpha \to 0$. For stable conditions to exist at all α, nonzero interfacial tensions and/or gravity are essential, and the density ratios need to favor the stability.

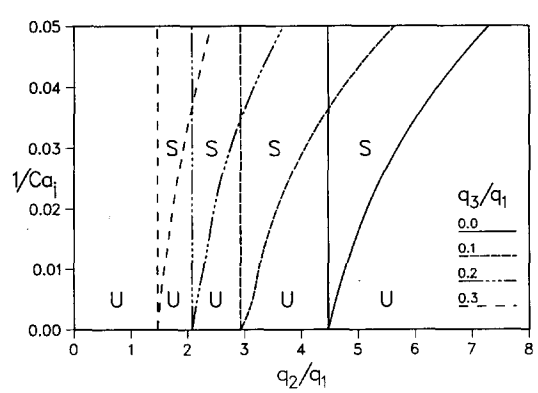

FIG. 11. Diagrams of stable conditions at *all* α for three-layer flow in the $1/Ca_j$-q_2/q_1 plane for various q_3/q_1. The other parameters are the viscosity ratios $m_2 = 20.0$ and $m_3 = 1.0$, the density ratios $d_j = 1.0$, $\mathrm{St} = 0.0$, and $\mathrm{Re}_1 = 5.0$. The stable and unstable regions are denoted by S and U, respectively.

ACKNOWLEDGMENT

This research is being funded by a grant from the Dow Chemical Company, Midland, Michigan, whose support is gratefully acknowledged.

[1] C. D. Han, *Multiphase Flow in Polymer Processing* (Academic, New York, 1981).
[2] S. F. Kistler and L. E. Scriven, Int. J. Numer. Methods Fluids **4**, 207 (1984).
[3] T. C. Papanastasiou, C. W. Macosko, and L. E. Scriven, Int. J. Numer. Methods Fluids **6**, 819 (1986).
[4] A. R. Gemmel and N. Epstein, Can. J. Chem. Eng. **40**, 215 (1962).
[5] C. S. Yih, J. Fluid Mech. **27**, 337 (1967).
[6] S. G. Yiantsios and B. G. Higgins, Phys. Fluids **31**, 3225 (1988).
[7] A. P. Hooper, Phys. Fluids A **1**, 1133 (1989).
[8] A. P. Hooper and W. G. C. Boyd, J. Fluid Mech. **128**, 507 (1983).
[9] D. D. Joseph, M. Renardy, and Y. Renardy, J. Fluid Mech. **141**, 309 (1984).
[10] A. P. Hooper, Phys. Fluids **28**, 1613 (1985).
[11] Y. Renardy and D. D. Joseph, J. Fluid Mech. **150**, 381 (1985).

[12]Y. Renardy, Phys. Fluids **28**, 3441 (1985).
[13]Y. Renardy, Phys. Fluids **30**, 1627 (1987).
[14]A. P. Hooper and W. G. C. Boyd, J. Fluid Mech. **179**, 201 (1987).
[15]A. F. M. Akhtaruzzman, C. K. Wang, and S. P. Lin, J. Appl. Mech. **45**, 25 (1978).
[16]S. K. Wang, J. J. Seaborg, and S. P. Lin, Phys. Fluids **21**, 1669 (1978).
[17]C. E. Hickox, Phys. Fluids **14**, 251 (1971).
[18]A. E. Everage, Trans. Soc. Rheol. **17**, 629 (1973).
[19]J. H. Southern and R. L. Ballman, Appl. Polym. Symp. **20**, 175 (1973).
[20]B. S. Ng and W. H. Reid, J. Comput. Phys. **30**, 125 (1979).
[21]B. S. Ng and W. H. Reid, J. Comput. Phys. **58**, 209 (1985).
[22]A. Davey, J. Comput. Phys. **35**, 36 (1980).